Magnetic phase transitions in $PrMn_2O_5$: Importance of ion-size threshold size effects in RMn_2O_5 compounds (R = rare earth)

C. Doubrovsky,[1] G. André,[2] A. Gukasov,[2] P. Auban-Senzier,[1] C. R. Pasquier,[1] E. Elkaim,[3]
M. Li,[4] M. Greenblatt,[4] F. Damay,[2] and P. Foury-Leylekian[1]

[1]*Laboratoire de Physique des Solides, Université Paris-Sud, CNRS-UMR 8502, 91405 Orsay Cedex, France*

[2]*Laboratoire Léon Brillouin, CEA-CNRS UMR 12 91191 Gif-sur-Yvette Cedex, France*

[3]*Soleil synchrotron, 91191 Gif-sur-Yvette Cedex, France*

[4]*Department of Chemistry and Chemical Biology, Rutgers, The State University of New Jersey, Piscataway, New Jersey 08854, USA*

(Received 14 September 2012; revised manuscript received 26 October 2012; published 19 November 2012)

A detailed investigation of the thermodynamic, structural, and magnetic properties of high quality polycrystalline $PrMn_2O_5$ samples are presented. In contrast with members of the RMn_2O_5 family with smaller rare-earth ions, $PrMn_2O_5$ is not ferroelectric and does not undergo a transition to an incommensurate (q_x, 0, q_z) magnetic phase: It exhibits two magnetic transitions, corresponding to commensurate magnetic orderings at $T_1 = 25 \pm 1$ K and $T_2 = 18 \pm 1$ K. These two magnetic transitions are characterized by two orthogonal propagation vectors $q_1 = (\frac{1}{2},0,0)$ and $q_2 = (0,0,\frac{1}{2})$, respectively, which coexist below T_2. The refinement of the neutron data show that Mn^{3+} order primarily at T_1, following q_1; below T_2, the Mn^{4+} sublattice orders following q_2.

DOI: 10.1103/PhysRevB.86.174417 PACS number(s): 75.25.−j, 75.30.Et, 61.05.F−, 61.05.cf

Multiferroic compounds are of current interest because they can stabilize simultaneously different types of ferroic orders which are coupled, such as ferroelectricity and (anti)ferromagnetism. The magnetoelectric effect resulting from such a coupling is promising for potential applications in the spintronic field.[1] Among the different theoretical models that have been proposed to understand the origin of the magnetoelectric coupling in multiferroics, two are put forward: The antisymmetric Dzyaloshinskii-Moriya interaction between ordered spins,[2] which requires a noncollinear magnetic arrangement, like in $TbMnO_3$,[3] and the exchange striction, which has been proposed to explain the appearance of ferroelectricity in the collinear phase of RMn_2O_5 (R = rare-earth, Bi) compounds.[4,5] The latter system has been intensively studied, owing to the discovery in $TbMn_2O_5$ of a huge magnetoelectric coupling, allowing us to reversibly inverse the direction of the electric polarization by applying a magnetic field.[6] The originality of these oxides resides in both the frustrated geometry of their magnetic lattice, and the mixed oxidation states of the Mn ions, an additional degree of freedom which can induce unique ferroelectric phases.

RMn_2O_5 compounds crystallize in the centrosymmetric orthorhombic $Pbam$ space group.[7,8] There are two distinct crystallographic sites for Mn^{4+}(Mn1 at site $4f$) and Mn^{3+} (Mn2 at site $4h$), which are coordinated by six and five oxygens, respectively (see Fig. 1). Within the (a,b) plane, the structure can be described as dimers of edge-sharing $Mn^{3+}O_5$ square pyramids sharing corners with $Mn^{4+}O_6$ octahedra and forming a zig-zag chain along the a axis. There are three inequivalent magnetic superexchange paths in the (a,b) plane between Mn magnetic ions (see Fig. 1): J_3 and J_4 between Mn^{3+} and Mn^{4+} spins, and J_5 between two Mn^{3+} spins. The main contribution to these constants is the antiferromagnetic (AF) Mn-Mn superexchange interaction through a shared oxygen. J_5 is expected to be the dominant integral.[9] Loops of five nearest-neighbor Mn ions antiferromagnetically coupled via the J_i (J_i = 3,4,5) exchange interactions results in magnetic frustration. The displacement of the Mn^{3+} ions, releasing the magnetic frustration by exchange striction and breaking the inversion symmetry (in particular the a glide plane symmetry), is suggested to explain the appearance of a polarization along the b direction in RMn_2O_5 compounds.[4,10,11] Along the c direction, $Mn^{4+}O_6$ octahedra share edges to form ribbons (see Fig. 1). In between the Mn^{4+} layers, layers of Mn^{3+} and R^{3+} alternate, so that there are two relevant Mn^{4+}-Mn^{4+} exchange interactions, J_2 (through the Mn^{3+} layers) and J_1 (through the R^{3+} layers) [Fig. 1(b)]. The main contribution to J_2 being the Mn^{4+}-Mn^{3+} superexchange coupling, J_2 is always ferromagnetic (F).[9,10]

A key issue in this series deals with the influence of the size of the rare-earth ion on the magnetoelectric properties, and, in particular, its effect on the Mn magnetic orderings through the J_1 magnetic exchange interaction. Interestingly, RMn_2O_5 compounds with a small R size (from R = Tb to R = Yb) all present similar behaviors, characterized by antiferromagnetic ordering at low temperature, about 40 K, with a propagation vector of the type (q_x, 0, q_z);[12–14] a series of magnetic transitions to commensurate and incommensurate magnetic phases is observed upon further cooling, concomitantly with ferroelectricity, polarization values being the largest in the commensurate phases.[15,16] The component of the propagation vector along c depends on the R size, and is extremely sensitive to interlayer coupling. For RMn_2O_5 compounds with larger R^{3+} ions, there is a unique antiferromagnetic transition, with a commensurate propagation vector corresponding to an AF coupling of the spins along the c direction, for instance, $q_M = (0,0,\frac{1}{2})$ for R = La[17] and $q_M = (\frac{1}{2},0,\frac{1}{2})$ for R = Bi.[18] To further investigate the influence of the size of the rare earth on the magnetoelectric properties of RMn_2O_5, studying intermediate R^{3+} sizes such as R = Pr, Nd is necessary. Such information is however lacking due to the difficulty of synthesizing high quality samples. In this article we thus present a comprehensive study of the structural, magnetic, and dielectric properties of high quality polycrystalline $PrMn_2O_5$, investigated by physical properties measurements combined with synchrotron radiation and neutron diffraction

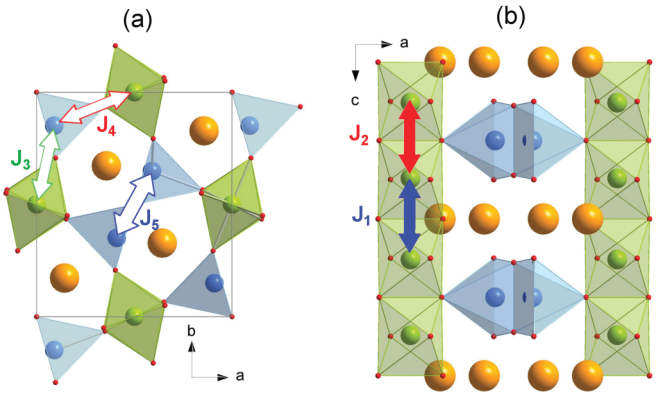

FIG. 1. (Color online) Projections of the crystal structure of $R\mathrm{Mn_2O_5}$ along (a) c and (b) b. The different J_i exchange interactions are indicated.

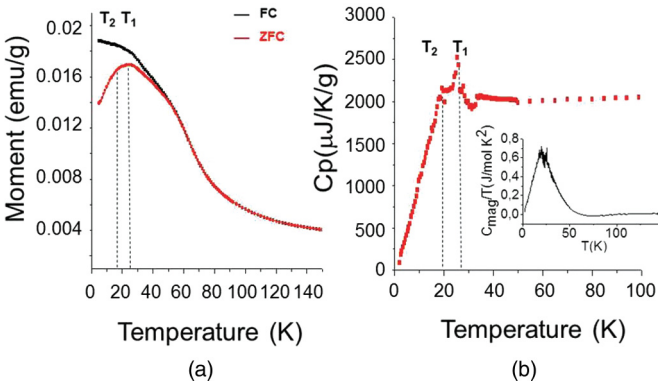

FIG. 2. (Color online) (a) Temperature dependence of the magnetization of $\mathrm{PrMn_2O_5}$ in 100 G. (b) Heat capacity vs temperature curve of $\mathrm{PrMn_2O_5}$. In the inset, magnetic contribution extracted from the experimental curve.

experiments. Although results of neutron diffraction (NPD) studies on $\mathrm{PrMn_2O_5}$ have been published recently,[19] a different interpretation of NPD data is given here.

High purity polycrystalline samples of $\mathrm{PrMn_2O_5}$ were synthesized from a precursor-based flux, following a method detailed in Refs. 7 and 20. Stoichiometric amounts of $\mathrm{Pr_6O_{11}}$ and $\mathrm{MnCO_3}$ were dissolved in 0.5 M citric acid and appropriate proportions of nitric acid while heating and stirring. The resulting solution was evaporated to a sol-gel and then fully dried in an oven at 130 °C. The obtained powder was fired at 600 °C for 12 h in air to obtain the precursor. The precursor was then mixed with $\mathrm{KClO_3}$ in a 1 to 7 ratio (weight based), and placed inside an $\mathrm{Al_2O_3}$ crucible before a final calcination at 850 °C for 24 h in air (heating and cooling rate of 150 and 300 °C/h, respectively). After reaction, the remaining KCl was washed away in water. Tiny $\mathrm{Mn_2O_3}$ and $\mathrm{Pr_2O_3}$ impurities were removed with either dilute (10%) hydrochloric or nitric acid.

The heat capacity, magnetic susceptibility, and dielectric constant experiments have been performed on powder samples compressed into pellets. Heat capacity has been measured with a physical properties measurements system (PPMS, Quantum Design). Magnetic susceptibility measurements were carried out using a commercial SQUID under zero-field cooling (zfc) and field cooling (fc) conditions. Dielectric constant was measured with a RLC bridge (HIOKI 5322) by applying a fixed voltage of 1 V at 5 kHz, using a homemade shielded sample holder. Synchrotron radiation diffraction experiments were performed on the CRISTAL beamline at the Soleil synchrotron light source (Saint-Aubin, France), with a two-circle diffractometer with 21 analyzer crystals to improve the angular resolution. A short x-ray wavelength of 0.48 Å was chosen to reduce absorption effects. The experiment was performed between $2\theta = 0°$ and 50° by step of 0.005°. Neutron powder diffraction experiments were carried out on a 5 g powder sample on the G4.1 diffractometer (Orphée-LLB, CEA-Saclay, France), with a neutron wavelength of 2.42 Å. Refinements of the crystal and magnetic structures were performed with the FULLPROF program.[21] Preliminary neutron scattering experiments on a single crystal have been performed on the 6T2 four circle diffractometer (Orphée-LLB), at a 0.9 Å wavelength.

The thermodynamic and magnetic characterizations (see Fig. 2) of the sample have been reported in Ref. 20. The heat capacity data indicate the presence of two phase transitions at $T_1 = 25 \pm 1$ K and $T_2 = 18 \pm 1$ K. The low temperature transition accounts for a weaker effect, observable over a broad temperature range [see Fig. 2(b)], in agreement with recent results.[19]

The magnetization curves exhibit a Curie-Weiss behavior above 50 K, with a Curie constant of 1.46×10^{-2} emu K g^{-1} Oe^{-1}, leading to a mean effective paramagnetic moment of $\approx 4.1\ \mu_B$, in excellent agreement with the value obtained averaging the effective paramagnetic moments of Mn^{4+}, Mn^{3+}, and Pr^{3+} ions. The zfc susceptibility measurements also evidence a decrease of χ in the T_1-T_2 range, an indication of the antiferromagnetic character of the T_1 phase transition [see Fig. 2(a)].

The thermal dependence of the dielectric constant (ϵ') has been measured at 5 kHz from room temperature to 10 K (see Fig. 3). In this temperature range, no ferroelectric transition has been detected and the system remains paraelectric. Pyroelectric measurement using an electric field of $E = 4$ kV cm^{-1} have confirmed the absence of electric polarization above 4.2 K. The $\epsilon'(T)$ curve also shows a weak steplike

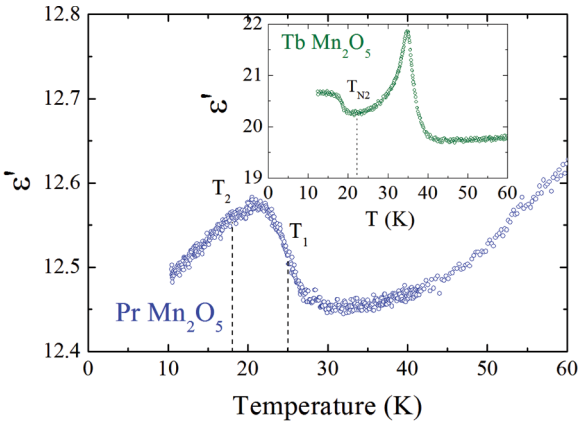

FIG. 3. (Color online) Thermal dependence of the real part of the dielectric constant at 5 kHz of $\mathrm{PrMn_2O_5}$ (main panel) and $\mathrm{TbMn_2O_5}$ (inset).

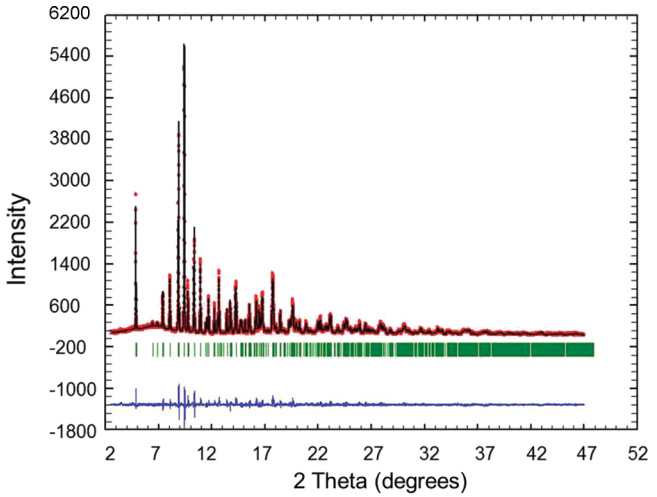

FIG. 4. (Color online) Rietveld refinement (experimental data: open circles, calculated profile: continuous line, allowed Bragg reflections: vertical marks). The difference between the experimental and calculated profiles is displayed at the bottom of the graph of the crystal structure of $PrMn_2O_5$ at 4 K.

increase below T_1. For comparison, the same measurement has been performed on a powder of the well-known multiferroic $TbMn_2O_5$ compound. The $\epsilon'(T)$ curve obtained, presented in the inset of Fig. 3, is very similar to the one previously published.[22] A sharp peak of ϵ' is observed at the ferroelectric transition T_E, and is followed by a steplike increase below $\approx T_{N2}$, similar to the one observed in $PrMn_2O_5$. This steplike anomaly in $\epsilon'(T)$ is frequently observed in RMn_2O_5 compounds (R = Er, Ho, Y, Dy, Tb, Gd, Eu[23]). Its origin is attributed to an electromagnon excitation characteristic of multiferroic systems, which corresponds to a phonon active mode coupled to a magnon excitation. Interestingly, within the RMn_2O_5 series, the observation of the steplike $\epsilon'(T)$ anomaly seems to be correlated with the transition into the noncollinear spin state.[22]

Figure 4 presents the synchrotron x-ray diffractograms obtained on the $PrMn_2O_5$ sample at 4 K, below the successive transitions. No symmetry lowering with respect to the centrosymmetric *Pbam* 300 K space group has been detected at low temperature. Refinement results of the 4 K structure show (see Table I) that there is no significant variation in the positions of the Mn and Pr species, when comparing with the

TABLE I. Rietveld refinement results of the crystal structure of $PrMn_2O_5$ at 4 K. Space group *Pbam*; $a = 7.5256(3)$ Å, $b = 8.6280(3)$ Å, $c = 5.6967(5)$ Å. Agreement factors: $R_{\text{Bragg}} = 2.61\%$, $\chi^2 = 1.71\%$.

Atom	Site	x	y	z	B_{iso}
Pr	4*g*	0.1428(9)	0.1720(8)	0	0.34(5)
Mn(1)	4*f*	0	0.5	0.2590(5)	0.22(8)
Mn(2)	4*h*	0.4095(3)	0.3501(4)	0.5	0.28(4)
O(1)	4*e*	0	0	0.2811(1)	0.24(8)
O(2)	4*g*	0.1564(1)	0.4482(3)	0	0.24(8)
O(3)	4*h*	0.1613(0)	0.4362(5)	0.5	0.24(8)
O(4)	8*i*	0.4002(4)	0.2030(3)	0.2473(6)	0.24(8)

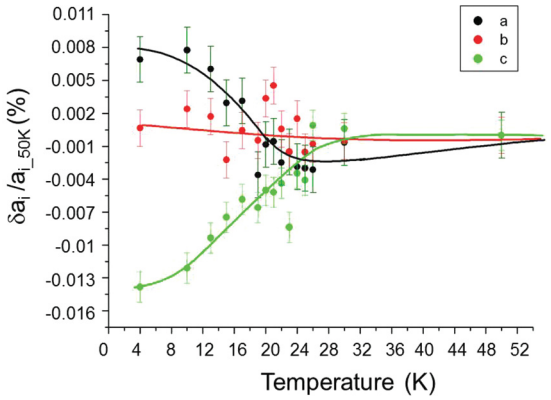

FIG. 5. (Color online) Relative temperature dependence of the unit cell parameters $[(a_i - a_{i50\,\text{K}})/a_{i50\,\text{K}}]$ of $PrMn_2O_5$, with respect to their 50 K values (from synchrotron x-ray diffraction data). Lines are guides to the eyes.

300 K structure previously published.[8,24] The thermal variation of the lattice parameters extracted from the refinement of the synchrotron data is presented in Fig. 5. The curves show that when cooling below $\approx 25 \pm 2$ K, that is, close to the magnetic transition temperatures, the a lattice parameter increases [$a(T)$ changes by 0.015% between 50 and 4 K], while c decreases; along b no change is observed in this temperature range. This result seems to point out a weak magnetoelastic coupling at the onset of the magnetic order in $PrMn_2O_5$. The absence of lattice distortion within the experimental resolution of the synchrotron x-ray experiment, contrasts with the smaller R compounds of this series. Indeed, in $TbMn_2O_5$, superstructure reflections at twice the magnetic wave vector have been observed and were associated with a strong magnetostriction effect.[13] It is also interesting to note that the thermal variation of the unit cell parameters of $PrMn_2O_5$ is similar to the one reported for $LaMn_2O_5$.[17]

The powder neutron diffraction study has been performed in the temperature range 30–2 K, by step of 1–2 K, as illustrated in Fig. 6. Below T_1 (≈25 K), antiferromagnetic Bragg

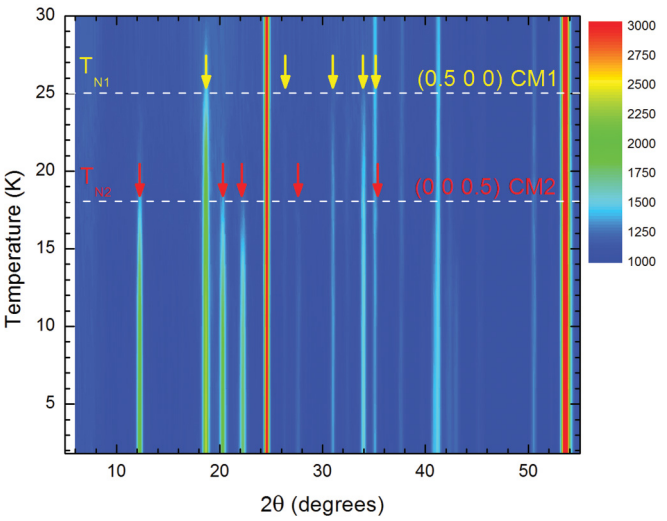

FIG. 6. (Color online) Powder neutron diffractograms (G4.1) of polycrystalline $PrMn_2O_5$ as a function of temperature.

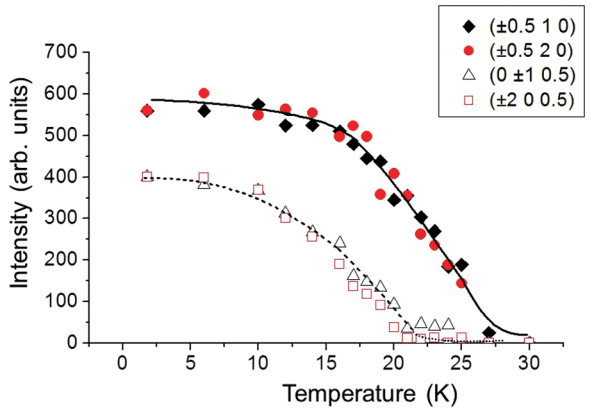

FIG. 7. (Color online) Temperature dependence of the integrated intensity of several magnetic reflections of $PrMn_2O_5$. Solid and dotted lines are guide for the eyes.

peaks appear, which can be indexed with the commensurate propagation vector $q_1 = (\frac{1}{2},0,0)$. The position of the magnetic peaks does not change with further cooling which confirms the commensurate character of the propagation wave vector.

Below T_2 ($\approx$18 K), a new set of magnetic Bragg peaks appear. They can be readily indexed with a commensurate propagation vector $q_2 = (0,0,\frac{1}{2})$. Like for q_1, the commensurability of the components of q_2 is sustained by the absence of any thermal variation of the Q position of the magnetic reflections. Below T_2, both q_1 and q_2 propagation vectors coexist, in agreement with Ref. 19. The evolution with temperature of the intensity $[I(T)]$ of the $(0,1,0) \pm q_1$ and $(0,2,0) \pm q_1$ magnetic reflections is represented in Fig. 7. This quantity, proportional to the square of the magnetic order parameter, increases monotonically when cooling below T_1 as expected for a second-order transition. No anomaly is detected at T_2 on the $I(T)$ curve. This indicates that the magnetic structure (CM1), which progressively establishes below T_1, is not affected by the T_2 transition. This behavior is not standard for a RMn_2O_5 compound. Indeed, for $TbMn_2O_5$, the temperature dependence of the intensity of the incommensurate magnetic peaks is strongly modified at the critical temperature of the successive phase transitions,[16] because these transitions involve a rearrangement of the magnetic moment of the same atoms.

The thermal evolution of the integrated intensity of the $(0, \pm1,0) + q_2$ and $(\pm2,0,0) + q_2$ reflections is also represented in Fig. 7. The $I(T)$ curves present a very slow increase between T_1 and T_2. Below T_2, the intensity then develops steadily and monotonically until $\frac{T_2}{2}$ and reaches a plateau at low temperature, as expected for the order parameter of a second-order phase transition. This result suggests that the second magnetic order (CM2) is initiated at the T_1 transition but that its real critical temperature is T_2.

Although the magnetic structures of $PrMn_2O_5$ are commensurate, their determination from neutron powder diffraction data is delicate owing to: First, weak magnetic reflections overlapping with crystal contributions, and second, to the 12 magnetic atoms, distributed on three different magnetic sublattices, Mn^{4+}, Mn^{3+}, and Pr^{3+}, and whose contributions in the successive magnetic orderings cannot be easily established.

The determination of the magnetic structure of the CM1 phase at 20 K will be presented first. A symmetry analysis has been performed with the BASIRREPS program[21] to find the irreducible representations of the little group G_k, which correspond to the symmetry elements of the $Pbam$ space group that leave the propagation vector $k = (\frac{1}{2}00)$ invariant. There are only two irreducible representations (IR), Γ_1 and Γ_2, but the crystal symmetry actually imposes very few constraints on the parameters to be determined, as, in particular, the four symmetrically equivalent Mn^{3+} and Pr^{3+} atoms are decoupled into pairs that can be coupled either in a ferromagnetic (F) or an antiferromagnetic (AF) fashion. For the Mn^{4+} site, Γ_1 IR corresponds to an antiparallel alignment of the in-plane components of the spins between successive Mn^{4+} ions along the c axis, while the Γ_2 one corresponds to a parallel alignment of the in-plane components of these spins. To reduce the number of variables, moments have been initially constrained to be collinear, and to lie within the (a,b) plane, as previously proposed for compounds of the same series.[14] Magnetic moments for ions on the same crystallographic sites have also been constrained to be identical.

The Rietveld refinement of the 20 K neutron diffraction pattern has been performed testing different models accordingly. A striking point is that most of the observed magnetic intensity can be accounted for by the ordering of the Mn^{3+} only, along the a axis. This Mn^{3+} ordering follows the Γ_2 IR. Two basis vectors underlie this configuration, which can be described as an AF coupling of the Mn^{3+} in (x,y,z) and $(-x,-y,z)$, along with a F coupling of the Mn^{3+} on sites $(-x+\frac{1}{2},y+\frac{1}{2},-z)$ and $(x+\frac{1}{2},-y+\frac{1}{2},-z)$. The ordered Mn^{3+} moments reach 1.59(6) μ_B at 20 K. The fact that the magnetic moments are aligned along the a axis is in good agreement with preliminary SQUID susceptibility measurements performed on a $PrMn_2O_5$ single crystal recently synthesized following[24] which indicate an easy axis along the a direction. Introducing a moment on the Mn^{4+} sites does not lead to any improvement of the refinement; within the experimental resolution, if Mn^{4+} do order, their moments remains small, less than about 0.4 μ_B, and would be coupled ferromagnetically along c, according to the Γ_2 IR, as already reported for other members of the series.[14] Surprisingly, in this 20 K magnetic phase, a partial ordering of the Pr^{3+} moment is observed. The Pr^{3+} moments are found parallel to their nearest-neighbor Mn^{3+} spins as aligned in their crystal field. Although the refined moment value of Pr^{3+} is small, about 0.50(7) μ_B, it undoubtedly improves the modeling of the data, leading to a decrease of the magnetic R_{Bragg} agreement factor by several percent. It is possible to further improve the refinement by releasing the collinear moment constraint, introducing a slight tilt of the Mn^{3+} moment with respect to the a axis, as noncollinearity is a known feature of small R members of the family.[10] This leads to a deviation of about 18° with respect to the a axis. This solution, which gives the best agreement with the experimental data, is presented in Fig. 8. Note here that in the q_1 magnetic structure proposed by Muñoz *et al.*,[19] Mn^{3+} and Mn^{4+} moments are equal, 1.8 μ_B at 1.5 K. Their model is, however, not compatible with our high quality data, as it leads to strong discrepancies between observed and calculated intensities on several magnetic Bragg reflections. At 1.5 K, the magnetic moments reach 1.97(5) μ_B for Mn^{3+} and 0.53(6) μ_B

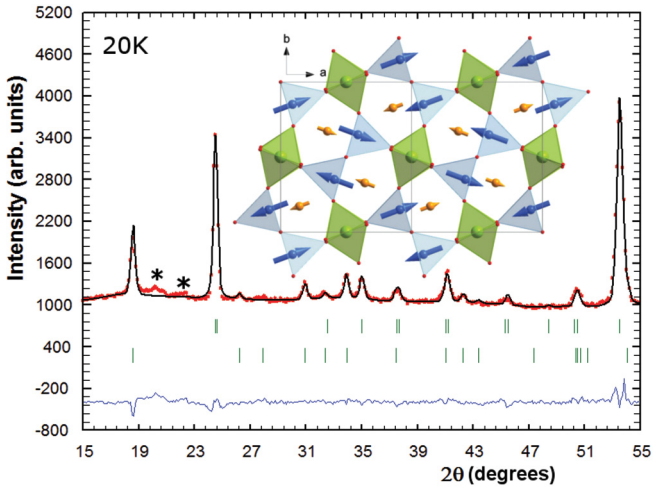

FIG. 8. (Color online) Rietveld refinement (experimental data: open circles, calculated profile: continuous line, allowed Bragg reflections: vertical marks). The difference between the experimental and calculated profiles is displayed at the bottom of the graph; the stars indicate weak reflections associated to the CM2 phase and magnetic structure of the CM1 20 K phase. There is no ordered moment on the Mn^{4+}.

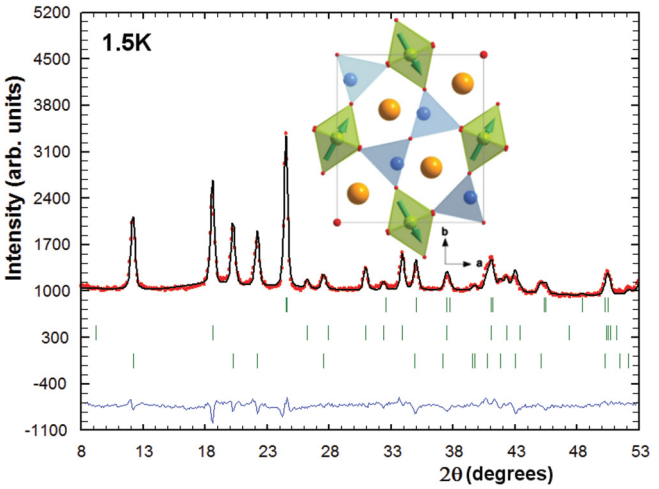

FIG. 9. (Color online) Rietveld refinement (experimental data: open circles, calculated profile: continuous line, allowed Bragg reflections: vertical marks). The difference between the experimental and calculated profiles is displayed at the bottom of the graph of the 1.5 K phase. In the inset is shown the magnetic ordering in the *ab* plane of the Mn^{4+} sublattice, following q_2 (CM2).

for Pr^{3+} (Table II). If ordered, the Mn^{4+} moment is less than 0.4 μ_B. These refined values are therefore still far from those expected at saturation (3, 4, and 2 μ_B for Mn^{4+}, Mn^{3+}, and Pr^{3+}, respectively). One can notice that in the other members of the RMn_2O_5 series, the ordered magnetic moments at low temperature are also far from their expected values for free ions.[18] Covalency effects are invoked to explain this effect. In our case, it is also important to notice that part of the magnetic moments can remain disordered because diffuse scattering is observed close to the magnetic reflections at low angle (Fig. 9).

Refinement of the q_2 magnetic structure is, as for the q_1 one, delicate, since in that case also, most of the magnetic scattering comes from the ordering of one sublattice, here Mn^{4+}. The representation analysis leads to stricter constraints than those obtained for q_1, however. The magnetic representation contains eight irreducible representations of dimension 1, details of which have been published in Ref. 19. The refinement

TABLE II. Rietveld refinement results of the magnetic structure of $PrMn_2O_5$ at 1.5 K. The components of the moment for each site in the primitive cell are given along the crystallographic directions (x,y,z), for the two propagation vectors $q_1 = (\frac{1}{2},0,0)$ and $q_2 = (0,0,\frac{1}{2})$. Magnetic R_{Bragg} agreement factor = 13.8%.

Atom	Moment	q_1	q_2
Mn^{3+}	M_x	−2.02(6)	0.27(4)
(0.411,0.351,0.5)	M_y	0.6(2)	0.0
	M_z	0.0	0.0
Mn^{4+}	M_x	0.0(4)	1.01(6)
(0,0.5,0.256)	M_y	0.0(2)	1.57(4)
	M_z	0.0	0.0
Pr^{3+}	M_x	−0.64(5)	0.0
(0.140,0.172,0)	M_y	−0.19(6)	0.0
	M_z	0.0	0.57(5)

results clearly show that at 2 K Mn^{4+} order following the Γ_6 IR: Successive Mn^{4+} along the *c* axis are coupled ferromagnetically on each side of the Mn^{3+} layer (in agreement with a ferromagnetic J_2), at the same *z*; the components of the moments along *b* are arranged antiferromagnetically (Fig. 9). The Mn^{4+} ordered moment reaches 2.0(2) μ_B at 1.5 K, and is rotated by about 57° with respect to the *a* axis. It is also necessary to add the refinement contributions from the two other magnetic lattices to get a satisfying agreement with the experimental data; to restrain the problem, only solutions within the same Γ_6 IR were investigated. The best agreement with the data is obtained for a weak ferromagnetic component along *a* on the Mn^{3+} sites (≈0.3 μ_B), and for pairs of AF coupled Pr^{3+} (≈0.6 μ_B along *c*). This therefore means that below T_2, Mn^{3+} and Pr^{3+} sublattices have components following both q_1 and q_2: In the case of Mn^{3+}, this leads to a slight modulation of the moment amplitude, which is larger when the coupling with the Mn^{4+} is ferromagnetic. For Pr^{3+}, the components of the magnetic moments following q_1 and q_2 being orthogonal, there is no modulation of amplitude, but of direction. As mentioned before, the moments on the two Mn^{3+} and Pr^{3+} sublattices are rather weak, which makes their determination from powder data delicate. As a result, although it leads to a satisfying refinement of the data (Fig. 9), the model proposed here might not be unique, in particular if mixtures of IR are involved. At this stage, a detailed single-crystal study is therefore essential to conclusively understand the role of Mn^{3+}, Mn^{4+} and Pr^{3+} in the two magnetic transitions.

Understanding the origin of this magnetic structure exhibiting two orthogonal magnetic propagation vectors remains challenging. Up to now, in the RMn_2O_5 series of compounds, the high temperature magnetic transition is mainly associated with the magnetic ordering of the Mn moments, independently of their oxidation state. The additional low temperature transitions correspond to a rearrangement of the Mn moments and/or the ordering of the R^{3+} moments in the

Mn crystal field. In contrast with the interpretation of Ref. 19, experimental evidences that $PrMn_2O_5$ exhibits two transitions, and that both occur in the same crystallographic domain are clear: (i) A weak coupling between the order parameters of both transitions is observed and (ii) the two transitions are systematically observed with the same relative intensity in all the samples studied,[19] (iii) a similar behavior is also observed in preliminary measurements of a $PrMn_2O_5$ single crystal.

The results tend to show that the main contribution to the T_1 transition is due to the Mn^{3+} moments ordering (and to a lesser extent to the Pr^{3+} ones), while the T_2 transition involves mostly the ordering of the Mn^{4+} moments. The total decoupling between the Mn^{3+} and Mn^{4+} spin orderings is not usual for this series of compound. However, it is observed in the prototype compound $TbMn_2O_5$[25] as well as in $ErMn_2O_5$[26] that the contribution of the Mn^{4+} moments becomes really sizable only a few degrees below the ordering of the Mn^{3+} moments. A total decoupling of the Mn^{3+} and Mn^{4+} spin orderings is also established in $EuMn_2O_5$.[27] A possible interpretation of this decoupling in $PrMn_2O_5$ is a valence modification of the Pr ions to a Pr^{4+} state below T_2. In that case the Mn1 atoms formally in a Mn^{4+} state and weakly ordered at the T_1 transition, become $Mn1^{3+}$. The magnetic coupling between the Mn1 ions via J_1 would thus be improved leading to their ordering. Simultaneously, the $Mn1^{3+}$-Pr^{4+}-$Mn1^{3+}$ exchange paths would be weakened due to the loss of $4f$ electrons on the Pr ion. Both effects would result in the AF order between Mn1 spins coupled by J_1 and thus a global AF order of the Mn1 (the alignment between Mn1 spins through J_2 is always F). Further work is in progress to determine the valence state of Pr by a x-ray absorption near edge spectroscopy (XANES) analysis at the Pr M4–5 edge.

In $PrMn_2O_5$, the Mn^{3+} configuration in the ab plane is similar to the one observed for all other members of the family, from $TbMn_2O_5$ to $YbMn_2O_5$. Mn^{3+} layers are, however, stacked ferromagnetically along c, in contrast to the q_z component characterizing smaller R compounds. In addition, in $PrMn_2O_5$, Mn^{4+} layers are coupled antiferromagnetically through the Pr^{3+} layer: In smaller R RMn_2O_5 compounds, the $(q_x, 0, q_z)$ vector implies a modulation of the amplitude of the moment on the R layer, which is not observed here, and which results in an alternate AF and F coupling of both the Mn^{4+} and Mn^{3+} layers. In $PrMn_2O_5$, the large Pr^{3+} ion strongly increases the distance between Mn^{4+} through the Pr^{3+} layer in the c direction. In that case it seems that the coupling between the two Mn sublattices, through the Mn^{3+}-Mn^{4+} superexchanges (J_3 and J_4) for example, is much weaker, so that the q_z-like modulation disappears. A similar feature is observed in the other large R RMn_2O_5 compounds (R = La,Bi[17,18]). It is well established that a strong R size effect control the magnetic ground state in the RMn_2O_5 series.[28] Our results seem to indicate that a threshold size effect occurs in $PrMn_2O_5$.

In summary, this study has shown that $PrMn_2O_5$ presents two second-order magnetic transitions, associated with orthogonal commensurate propagation vectors $q_1 = (\frac{1}{2},0,0)$ and $q_2 = (0,0,\frac{1}{2})$. The dielectric measurements have shown that the compound is not ferroelectric. All these features differ from most other RMn_2O_5 compounds with magnetic R^{3+} ions, in which the magnetic order is first incommensurate, the ferroelectric phase appearing at the incommensurate to commensurate transition. This clearly evidences the strong impact of the nature of the rare earth on both the magnetic ground state and the emergence of the ferroelectric properties. Inelastic neutron diffraction and *ab initio* calculations are in progress to try to estimate and compare exchange constants in both $PrMn_2O_5$ and $TbMn_2O_5$ compounds.

We thank S. Petit, M. B. Lepetit, F. Bert, A. Cano, and A. Sazonov for very helpful scientific discussions.

[1] W. Eerenstein, N. D. Mathur, and J. F. Scott, Nature (London) **442**, 759 (2006).
[2] I. A. Sergienko and E. Dagotto, Phys. Rev. B **73**, 094434 (2006).
[3] M. Kenzelmann, A. B. Harris, S. Jonas, C. Broholm, J. Schefer, S. B. Kim, C. L. Zhang, S.-W. Cheong, O. P. Vajk, and J. W. Lynn, Phys. Rev. Lett. **95**, 087206 (2005).
[4] S. W. Cheong and M. Mostovoy, Nat. Mater. **6**, 13 (2007).
[5] H. Katsura, N. Nagaosa, and A. V. Balatsky, Phys. Rev. Lett. **95**, 057205 (2005).
[6] N. Hur, S. Park, P. A. Sharma, J. S. Ahn, S. Guha, and S-W. Cheong, Nature (London) **429**, 392 (2004).
[7] J. A. Alonso, M. T. Casais, M. J. Martínez-Lope, J. L. Martínez, and M. T. Fernández-Díaz, J. Phys.: Condens. Matter **9**, 8515 (1997).
[8] I. Kagomiya, K. Kohn, and T. Uchiyama, Ferroelectrics **280**, 131 (2002).
[9] M. B. Lepetit (private communication).
[10] P. G. Radaelli and L. C. Chapon, J. Phys.: Condens. Matter. **20**, 434213 (2008).
[11] L. C. Chapon, G. R. Blake, M. J. Gutmann, S. Park, N. Hur, P. G. Radaelli, and S-W. Cheong, Phys. Rev. Lett. **93**, 177402 (2004).
[12] G. Buisson, Phys. Status Solidi **16**, 533 (1973); **17**, 191 (1973).
[13] Y. Noda, H. Kimura, M. Fukunaga, S. Kobayashi, I. Kagomiya, and K. Kohn, J. Phys.: Condens. Matter **20**, 434206 (2008).
[14] G. R. Blake, L. C. Chapon, P. G. Radaelli, S. Park, N. Hur, S-W. Cheong, and J. Rodriguez-Carvajal, Phys. Rev. B **71**, 214402 (2005).
[15] P. Tolédano, W. Schranz, and G. Krexner, Phys. Rev. B **79**, 144103 (2009).
[16] J. Koo, C. Song, S. Ji, J.-S. Lee, J. Park, T.-H. Jang, C.-H. Yang, J.-H. Park, Y. H. Jeong, K.-B. Lee, T. Y. Koo, Y. J. Park, J.-Y. Kim, D. Wermeille, A. I. Goldman, G. Srajer, S. Park, and S.-W. Cheong, Phys. Rev. Lett. **99**, 197601 (2007).
[17] A. Muñoz, J. A. Alonso, M. T. Casais, M. J. Martínez-Lope, J. L. Martínez, and M. T. Fernández-Díaz, Eur. J. Inorg. Chem. **2005**, 685 (2005).
[18] A. Muñoz, J. A. Alonso, M. T. Casais, M. J. Martínez-Lope, J. L. Martínez, and M. T. Fernández-Díaz, Phys. Rev. B **65**, 144423 (2002).
[19] A. Muñoz, J. A. Alonso, M. J. Martínez-Lope, V. Pomjakushin, and G. André, J. Phys.: Condens. Matter **24**, 076003 (2012).

[20]C. Doubrovsky, G. Andre, F. Bouquet, E. Elkaim, M. Li, M. Greenblatt, and P. Foury-Leylekian, Physica B **407**, 1718 (2012).
[21]J. Rodriguez-Carvajal, Physica B **192**, 55 (1993).
[22]A. B. Sushkov, R. V. Aguilar, S. Park, S-W. Cheong, and H. D. Drew, Phys. Rev. Lett. **98**, 027202 (2007).
[23]A. B. Sushkov, M. Mostovoy, R. Valdés Aguilar, S.-W. Cheong, and H. D. Drew, J. Phys.: Condens. Matter **20**, 434210 (2008).
[24]G. Popov, M. Greenblatt, and W. H. McCarroll, Mater. Res. Bull. **35**, 1661 (2000).
[25]C. Wilkinson, P. J. Brown, and T. Chatterji, Phys. Rev. B **84**, 224422 (2011).
[26]P. P. Gardner, C. Wilkinson, J. B. Forsyth, and B. M. Wanklyn, J. Phys. C **21**, 5653 (1988).
[27]V. Polyakov, V. Plakhty, M. Bonnet, P. Burlet, L. P. Regnault, S. Gavrilov, I. Zobkalo, and O. Smirnov, Physica B **297**, 208 (2001).
[28]C. Ma, J. Q. Yan, K. W. Dennis, R. W. McCallum, and X. Tan, J. Solid Stat. Chem. **182**, 3013 (2009)